Development of a smart machine vision based system to detect water stress in greenhouse tomato plants

Mohammadbagher Lak[1], Saeid Minaei[1*], Saeid Soufizadeh[2], Ahmad Banakar[1], Gerrit Polder[3]

(1. Biosystems Engineering Department, Tarbiat Modares University, Tehran, Iran; P.O.B.: 14115-111
2. Department of Agroecology, Environmental Sciences Research Institute, Shahid Beheshti University, General Campus, Tehran, Iran;
3. Wageningen University & Research, Greenhouse Horticulture, Wageningen, Netherlands).

Abstract: Timely detection of water stress in agricultural crops is important. In this paper, a smart classification algorithm was developed to detect water stress in tomato plants that were grown in the greenhouse. During the growth period, thermal and visible light images were acquired from the canopy tops in two states: (1) plants in normal conditions; and (2) plants under water stress. Images were obtained using a camera that recorded simultaneous frames of thermal and visible (red, green, and blue (RGB)) features. Based on these features, 22 parameters were defined and applied to classify the image frames. In order to develop an efficient algorithm, principal component analysis (PCA) was applied to optimize the classifying of parameters. For normalizing the data in PCA, 6 normalization methods were applied and assessed. Among them, peak normalization was the best as its PC1 and PC2 described 94% and 5% of total variation, respectively. Based on the PCA results, 9 parameters were found with most loadings as the most effective indexes that all obtained from the visible features. In other words, the thermal features were not as useful for detecting plant water stress. These parameters were used in multilayer perceptron neural networks (MLPNN) to develop the classification algorithm. The resulting mean-square error and r values for the MLPNN with ten hidden layer were 6.05×10^{-3} and 0.9905, respectively which shows the robustness of the classification algorithm. This algorithm accuracy was 83.3%.

Keywords: image classification, MLPNN, normalization, PCA, precision farming

Citation: Lak, M., S. Minaei, S. Soufizadeh, A. Banakar, and G. Polder. 2021. Development of a smart machine vision based system to detect water stress in greenhouse tomato plants. Agricultural Engineering International: CIGR Journal, 23(2): 141-151.

1 Introduction

Water deficit is a result of transpiration with rates more than water uptake that causes inhibition of plant growth and development. Associated with this phenomenon, turgor pressure falls resulting in stomata closure (Blum, 2011; Wolf and Rudich, 1988). Closed stomata lead to decreased CO_2 assimilation rate and photosynthesis in plant leaves. Thus, absorbed irradiation energy cannot be used in photosynthesis (Katsoulas et al., 2016). This stress and the consequent reactions of plants lead to changes in leaf color and temperature (Lin et al., 2013) which may significantly reduce plant productivity (Kim et al., 2011). Therefore, early detection of water stress in plants is critical (Katsoulas et al., 2016) and automated real-time detection of plant stress would decrease losses (Kim et al., 2011).

Plant canopy temperature has been introduced as a good indicator for detection of plant water status (Wang et al., 2010). Therefore, several thermal indices based on remote infrared thermographic measurements were introduced by Bartzanas et al. (2015) for plant water

Received date: 2020-01-24 **Accepted date:** 2021-03-23

***Corresponding author: Saeid Minaei,** professor, Biosystems Engineering Department, Tarbiat Modares University, Tehran, Iran. Tel: +98 21 4829 2466. Email: minaee@modares.ac.ir.

stress detection in greenhouses. Wang et al. (2010) monitored the temperature difference between canopy and ambient as an indicator for monitoring water status in plants. Water status in apple trees was assessed by analyzing the spectral signature of plant leaves and the highest correlation between spectral indices and stress levels was found using red edge normalized difference vegetation index (NDVI) at 705 and 750 nm in narrowband indices and NDVI at 680 and 800 nm in broadband indices (Kim et al., 2011). In another study, water stress was monitored in non-homogeneous crop canopies of an olive garden using an airborne hyperspectral scanner acquiring imagery in 38 spectral bands in the 430–1250 nm spectral range (Sepulcre-Cantó et al., 2006).

In addition to spectral and thermal inspections, visible spectra have been utilized to detect water stress in agricultural crops in some works. Kacira et al. (2002) developed a machine vision system to detect water stress in New Guinea Impatiens by means of visible images. They measured top-projected canopy area and introduced the coefficient of relative variation of top–projected canopy area as a marker for stress detection (Kacira et al., 2002). Leaf deflection and associated stem and leaf inclination of tomato plants have also been measured as water stress indicators (Font et al., 2005).

Researchers have reported that applying hue-saturation-intensity (HIS) color space is sufficient and reliable to predict and classify water stress in Sunagoke moss plants (Ondimu and Murase, 2008). In a similar research, hue values of RGB images were successfully utilized for detecting disease stress in wheat (Casanova et al., 2014).

For real-time, nondestructive and non-contact detection of water stress in agricultural crops, a vast variety of sensor-based methods has been suggested a few of which were reviewed here. Among the developed machine-vision-based methods to detect water stress, thermal images have been used in many research works. This is while processing visible images is mostly devoted to image segmentation or color space conversions.

The objective of this paper is to develop an accurate and inexpensive machine-vision-based, classifying method to detect water stress in tomato plants using images in the visible wavelength range.

2 Material and methods

In order to develop a machine-vision-based smart classification system to distinguish normal and water-stressed tomato plants, they were grown under controlled conditions in a greenhouse at Tarbiat Modares University, Tehran, Iran (35.74°N, 51.16°E). Potted tomato plants (Solanum lycopersicum, cv. 'Early Ch.) were grown under the same conditions of soil volume, density, texture (loamy sand), and fertility; air temperature and humidity; as well as illuminance conditions throughout the greenhouse to mask the effect of undetermined factors (errors). Three different irrigation schedules were implemented to obtain normal (class 1) and water stressed (class 2) treatments. Thus, it was possible to take photos of both classes under uniform conditions to diminish the data collection errors.

As the soil texture was coarse, the plants were irrigated in close intervals (Heuvelink, 2005) including three treatments: once per 96 h (i1), 72 h (i2), and 48 h (i3). Depending on the irrigation schedule, it was assumed that the plants would face water stress during the period of 48 to 96 h after irrigation based on soil water content. During tomato growth and development, thermal and visible light images were acquired from the plant canopies, at two times: (1) 2 to 24 h after irrigation when plants were succulent; and (2) 48 to 96 h after irrigation when they were under reversible water stress.

Table 1 Camera technical specifications

Characteristics		Specifications
Visible Image	Color space	RGB
	Resolution	2.0 Megapixels
	Processor	CMOS
Thermal Image	Spectral range	800 to 1400 nm
	Thermal Sensitivity	≤0.08℃ at 30℃
	Temperature Range	-20℃ to 250℃
	Accuracy	2% of reading
	Operating Temperature	-10℃ to 50℃
	Operating Humidity	10% to 95%, non-condensing

The images were acquired under natural daylight conditions without any control or artificial lighting. The thermal and visible images were simultaneously acquired using an infrared camera (ITI-P400, Infrared

Thermography Inspection, Sweden). Specification of which are given in Table 1.

The camera was fixed on a stand that was linked to the top rails. The top rails consisted of two rails fixed to the top of the greenhouse structure (to guide the moving platform direction) and one moving rail (platform) was perpendicular to the fixed rails. The H-shaped rail system made it possible for the camera stand to cover all the plants throughout the length and width of the greenhouse, while the camera height could be adjusted through the stand length. Camera height was adjustable between 150 and 180 cm from the greenhouse floor (depending on the plant age) to acquire images with the same scale. This camera was able to record the visible and thermal images and combine them into one data matrix. Therefore, its visible and thermal images were recorded in one file ($f(x,y) = [r, g, b,$ Temperature]). Then, the images were transferred to the laptop and preprocessed using the camera interface (ITI-IrAnalyser) to export visible images and thermal properties from the raw images.

Among the thermal properties, maximum and minimum temperatures of each frame were measured. It was assumed that the emissivity of tomato leaves is 0.98 (López et al., 2012). Simultaneously, the visible images were also exported from the software. The visible images were acquired in RGB color space that consisting of red, green, and blue image matrixes. Maximum temperature (T_{max}) and minimum temperature (T_{min}) were obtained from the thermal images.

Intensity ($I = \frac{r+g+b}{3}$) and excessive green ($EG = 2g - r - b$) image matrices were extracted from the RGB images for further image processing according to Sabeenian and Palanisamy (2010). The minimum and maximum temperatures, extracted from the thermal images, as well as the visible characteristics were utilized as the parameters of image classification.

Five indexes were determined based on the thermal characteristics (Equations 1 to 5). Means and standard deviations for all the visible image matrices (*r, g, b, I,* and *EG*) were then determined and coefficients of variation were calculated (Equation 6).

$$Ind_1 = T_{max} - T_{min} \quad (1)$$

$$Ind_2 = \frac{T_{max}-T_{min}}{T_{max}} \quad (2)$$

$$Ind_3 = \frac{T_{max}-T_{min}}{T_{min}} \quad (3)$$

$$Ind_4 = \frac{T_{max}-T_{min}}{T_{max}+T_{min}} \quad (4)$$

$$Ind_5 = \frac{T_{min}}{T_{max}} \quad (5)$$

$$CV_m = \frac{SD_m}{Mean_m} \quad (6)$$

Where: T_{max} and T_{min} are the maximum and minimum temperatures, respectively (°C); CV_m is the coefficient of variation in each matrix; m implies any of image matrices r, g, b, i, or EG; SD_m is the standard deviation of each matrix; and $Mean_m$ is the mean of each matrix.

Based on the preprocessed and processed data, 22 parameters were determined for classifying the images into normal (class 1) and water-stressed (class 2) groups. These parameters included: T_{max}, T_{min}, Ind_1, Ind_2, Ind_3, Ind_4, Ind_5 (Equations 1 to 5), $Mean_r$, $Mean_g$, $Mean_b$, $Mean_i$, $Mean_{EG}$, SD_r, SD_g, SD_b, SD_i, SD_{gs}, CV_r, CV_g, CV_b, CV_i, and CV_{EG} (Equation 6).

3 Results and discussion

A large number of parameters increase the classifying computational complexity which reduces the feasibility of applying a classification algorithm (Park, 2011). Therefore, the parameters must be reduced. Principal components analysis (PCA) was used as an unsupervised approach that transforms a large multivariate dataset of measured original variables into a new space with linearly uncorrelated attributes called Principal components (PCs) using orthogonal transformation (Dinç et al., 2014). Here, PC1 explains the highest variance in the data and PC2 explains the next largest variance in the data. At first, PCA was run on the raw data (not normalized) of measured and calculated parameters (Figure 1).

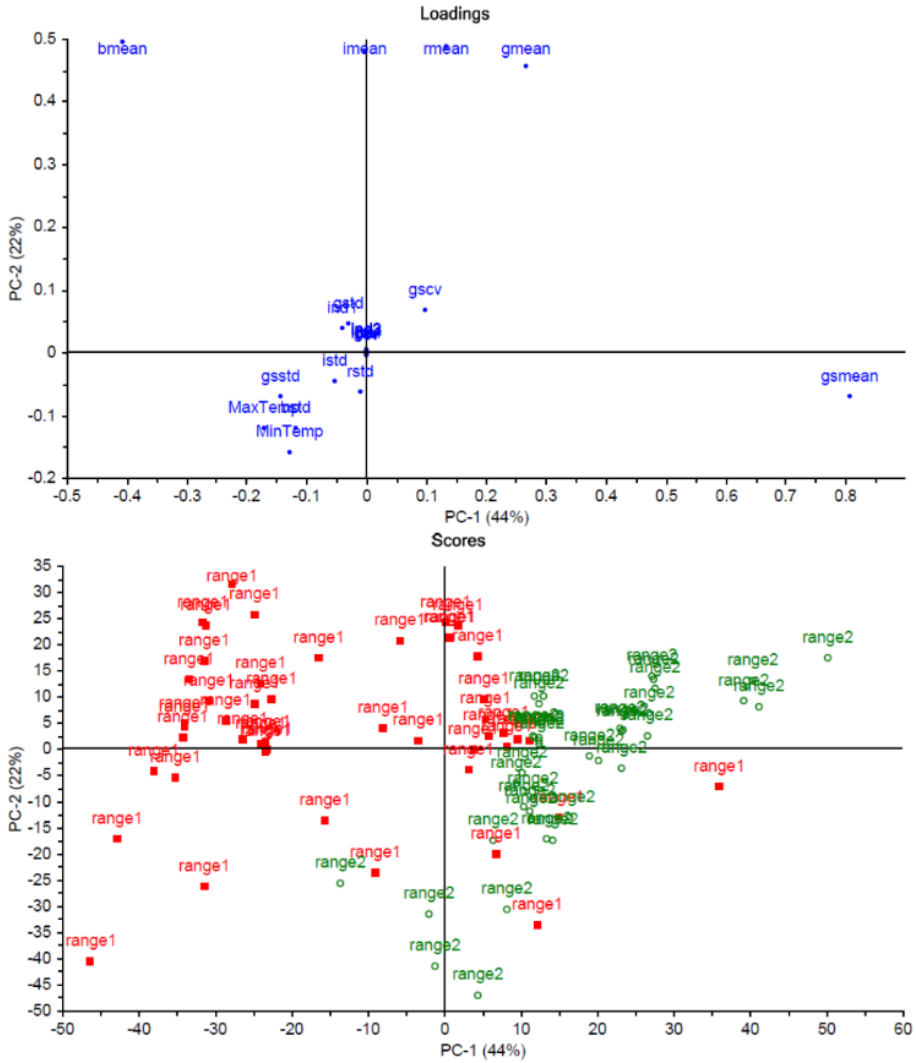

Figure 1. Results of running PCA on the raw data

(the inferior point graph, showing the cores, includes two classes: range 1 stands for succulent plants and range 2 for water-stressed)

As shown in Figure 1, PC1 describes 44% and PC2, 22% of the total variation when running the PCA on the raw data. PCs larger than 90% are more desirable (Holland, 2008). Therefore, the data was normalized to achieve more reliable PCs and consequently increase classification performance.

3.1 Normalization

Normalization, as a family of transformations, is utilized to scale the samples in order to get all the data on approximately the same scale. For this purpose, six normalization methods were applied and evaluated as follows. In order to apply the normalization methods, Unscrambler 10 software (Anonymous, 2010) has been utilized.

1) Area normalization divides an observation (X_i) by the area under the curve of observation ($\widehat{X}_i = \frac{X_i}{\sum_j x_{ij}}$). For all the samples ($X_i$), the area ($\sum_j x_{ij}$) becomes the same (Figure 2) (Anonymous, 2010).

2) Unit vector normalization, as a useful method in some pattern recognition applications, transforms the X_i to unit vector ($\widehat{X}_i = \frac{X_i}{\sqrt{\sum_j x_{ij}^2}}$) that results in samples with a norm of 1 (Anonymous, 2010). Results of raw data normalization using unit vector method are shown in Figure 3.

3) Mean normalization divides each row of data matrix by its average, thus, the influence of the hidden factor is negated and it keeps the area under the curve the same for all the samples (Figure 4) (Anonymous, 2010).

4) Maximum normalization, contrary to mean normalization, this method divides each row by its maximum absolute value. If all the sample values are positive, the maximum value becomes +1; conversely, if all the values are negative, the minimum value becomes -1 (Figure 5) (Anonymous, 2010).

5) In range normalization, each row is divided by its range ($X_{max} - X_{min}$). The curve span becomes 1 (Figure 6) (Anonymous, 2010).

6) Peak normalization normalizes a sample X_i divided by the chosen k^{th} data point, which is always selected for both the training set and the unknowns for prediction ($\widehat{X}_i = \frac{X_i}{x_{i,k}}$). The peak variable (max) is equal to the total number of variables and all the transformed samples take the value of 1 at the chosen constant point (Figure 7) (Anonymous, 2010).

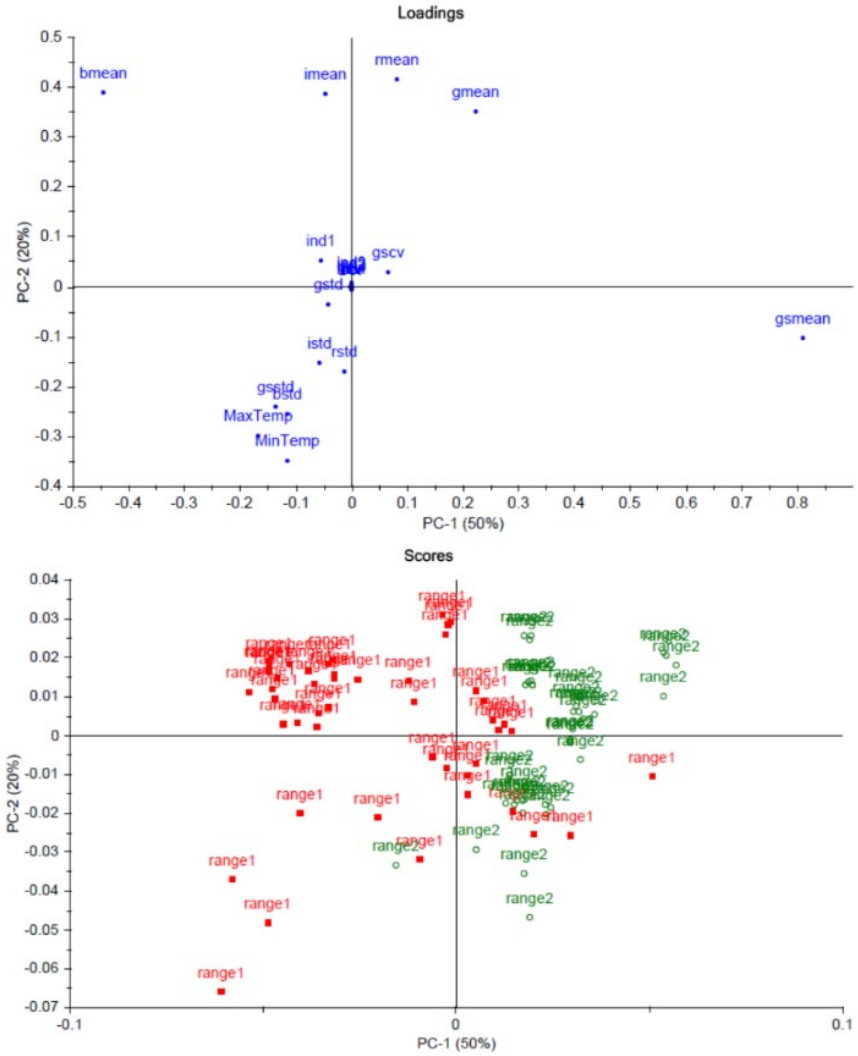

Figure 2. Results of running PCA on area-normalized data

(the inferior point graph, showing the cores, includes two classes: range 1 stands for succulent plants and range 2 for water-stressed)

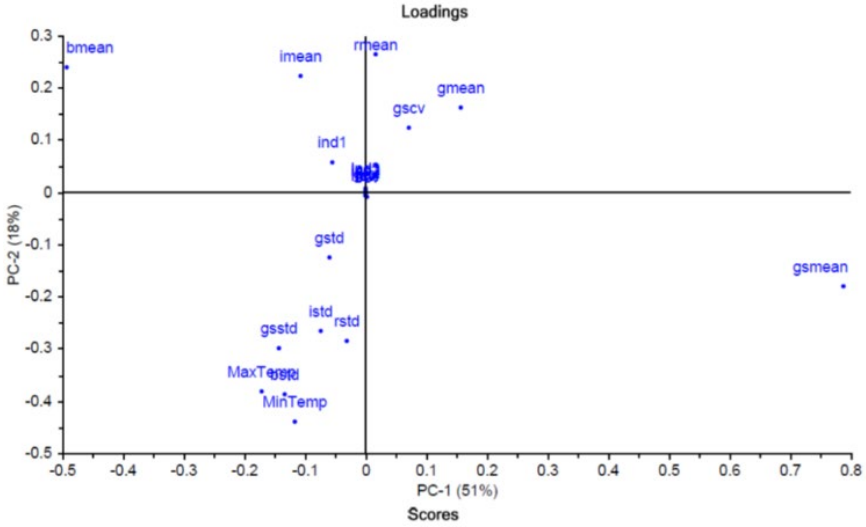

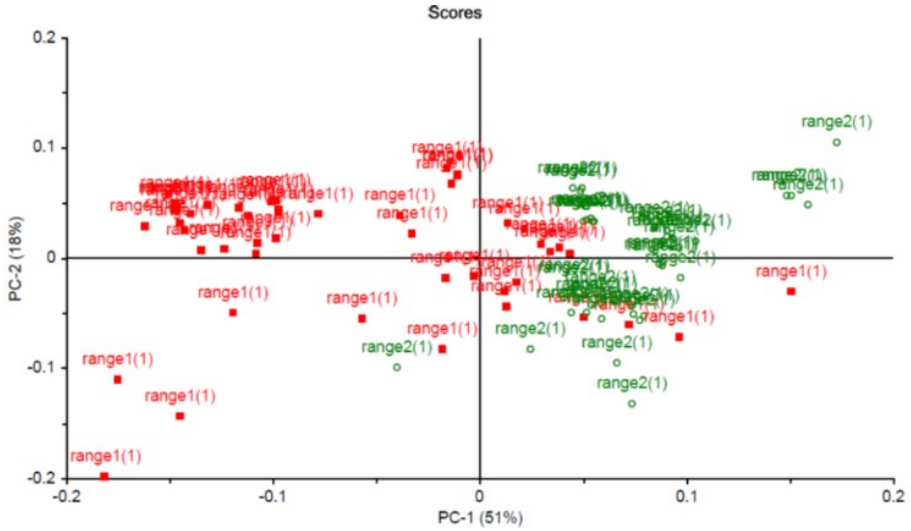

Figure 3. Results of running PCA on unit-vector-normalized data

(the inferior point graph, showing the cores, includes two classes: range 1 stands for succulent plants and range 2 for water-stressed)

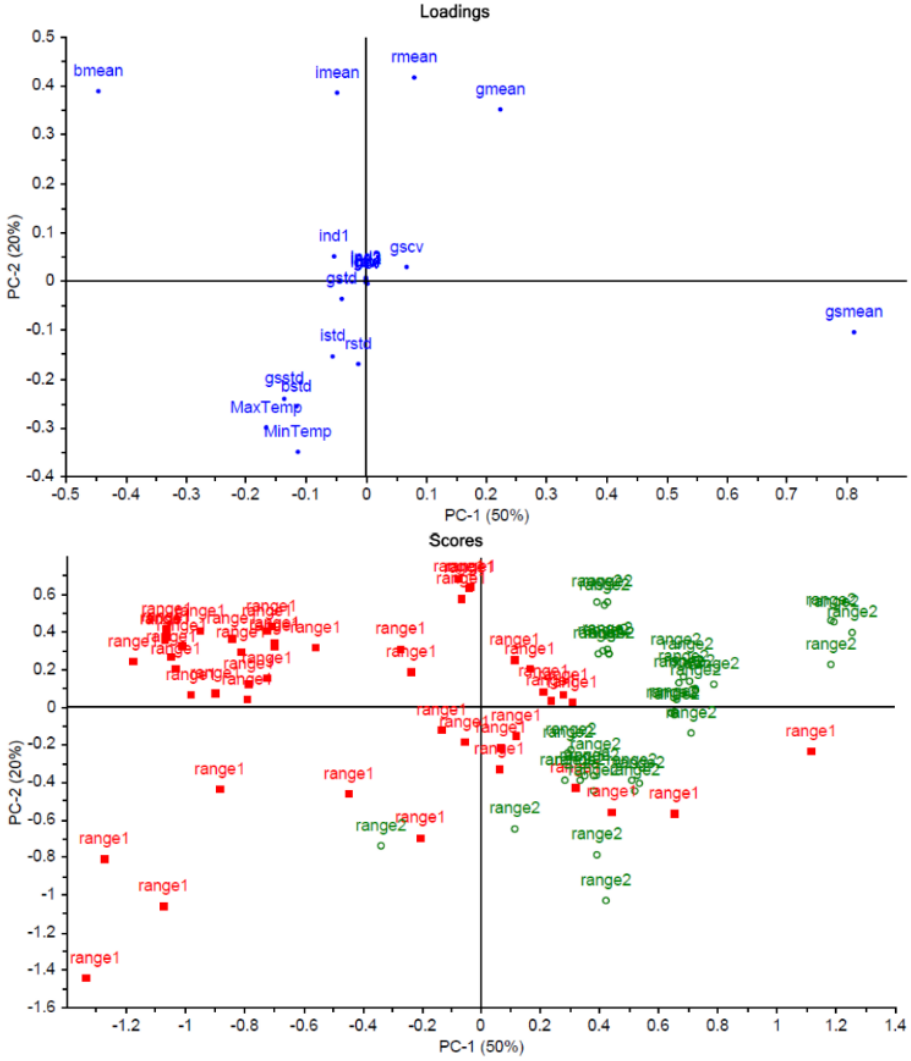

Figure 4. Results of running PCA on mean-normalized data

(the inferior point graph, showing the cores, includes two classes: range 1 stands for succulent plants and range 2 for water-stressed)

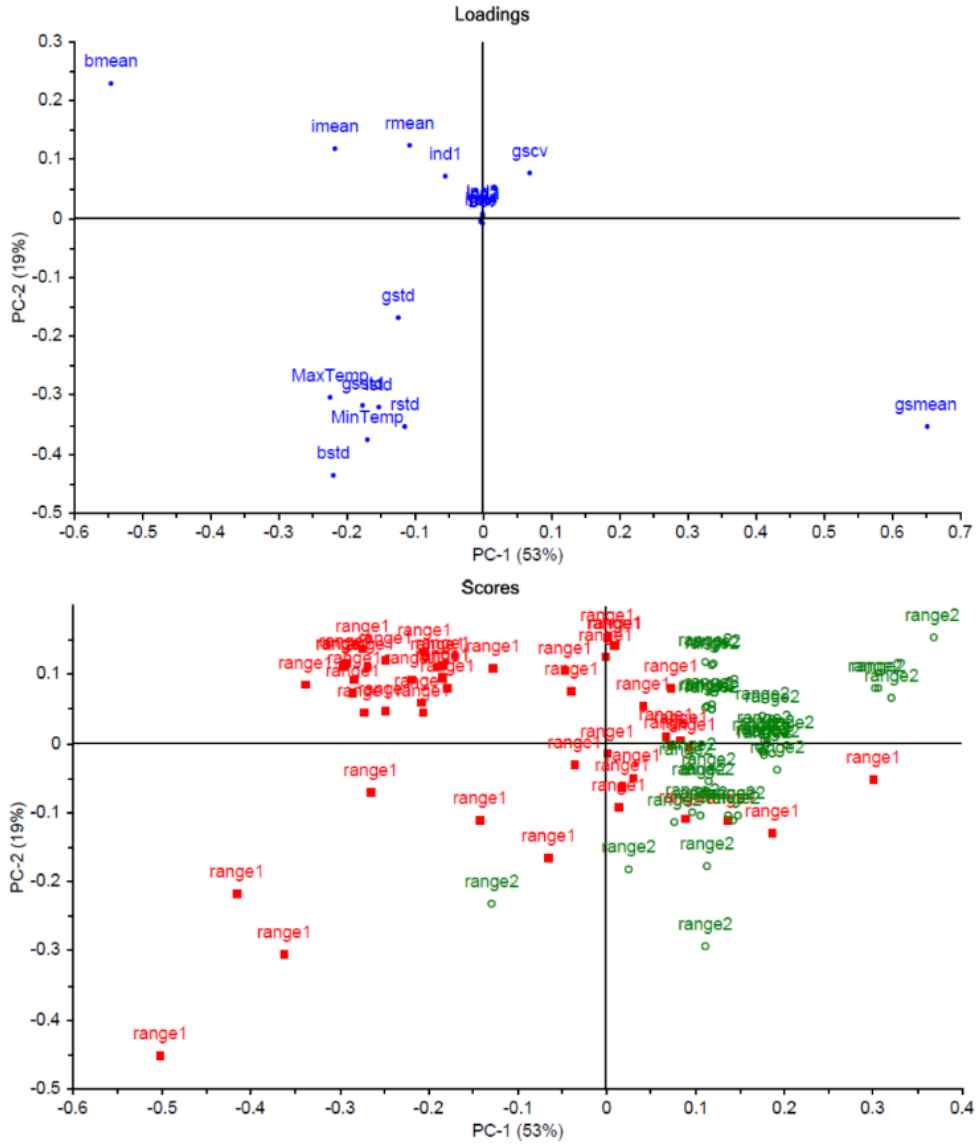

Figure 5. Results of running PCA on maximum-normalized data

(the inferior point graph, showing the cores, includes two classes: range 1 stands for succulent plants and range 2 for water-stressed)

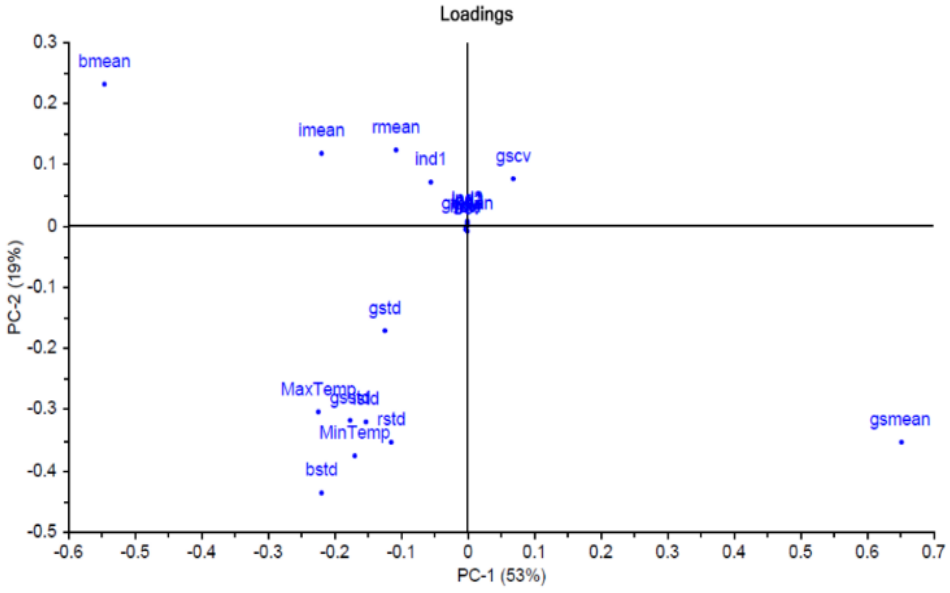

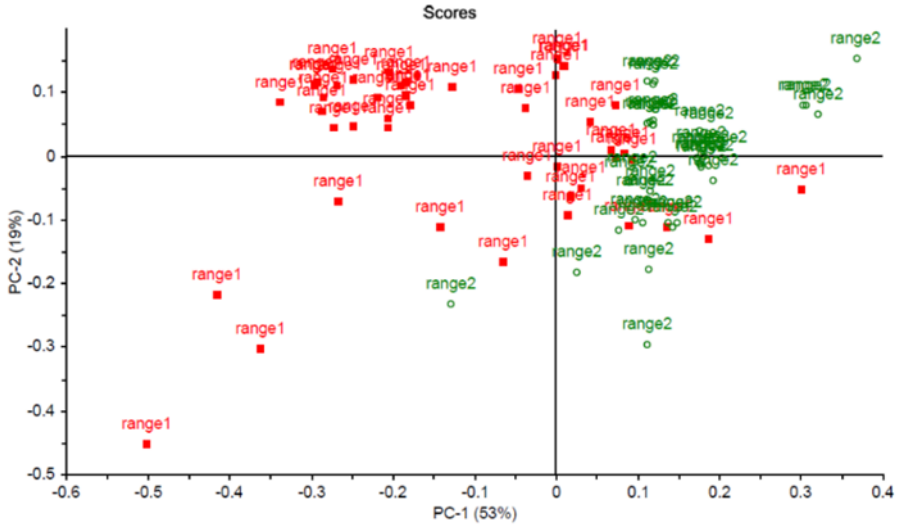

Figure 6. Results of running PCA on range-normalized data

(the inferior point graph, showing the cores, includes two classes: range 1 stands for succulent plants and range 2 for water-stressed)

As shown in Figures 1 to 6, for raw data (not normalized) and data normalized by area normalization, unit vector normalization, mean normalization, maximum normalization, or range normalization, their first two PCs (PC1 and PC2) ranged from 69% to 72% which is low and not desirable. Therefore, peak normalization was tested (Figure 7).

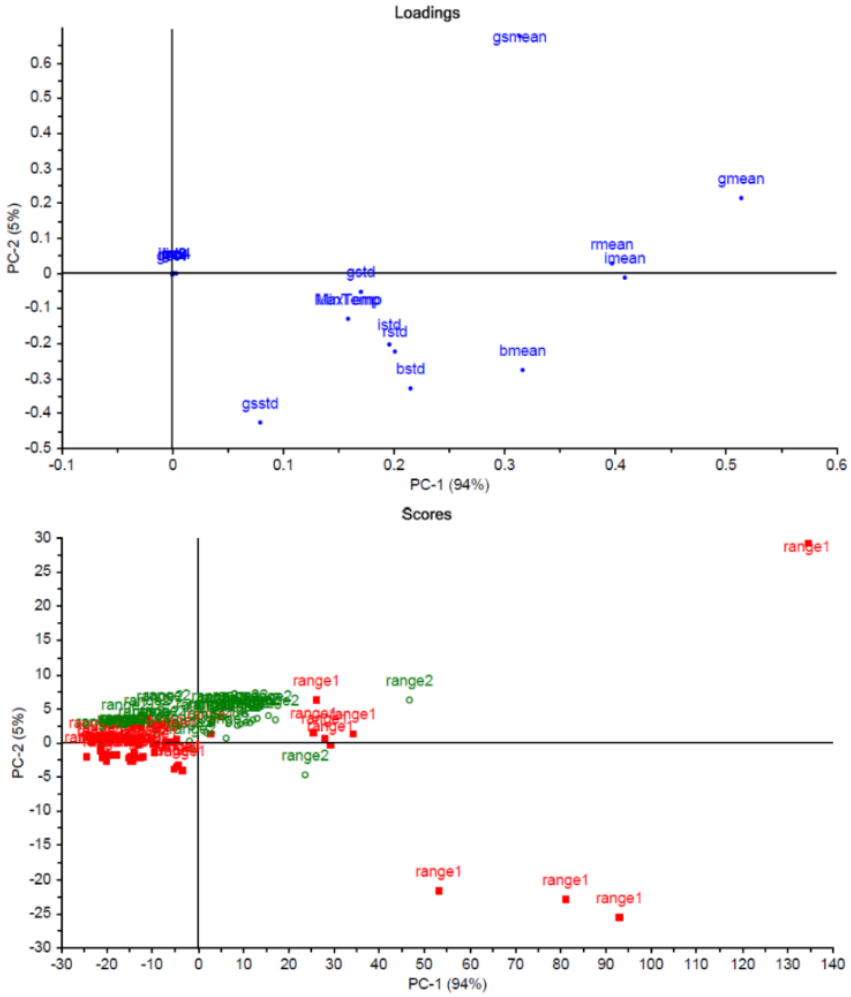

Figure 7. Results of running PCA on peak-normalized data

(the inferior point graph, showing the cores, includes two classes: range 1 stands for succulent plants and range 2 for water-stressed)

As shown in Figure 7, the first two PCs obtained by peak normalization together account for 99% of data variance of the original dataset. This fact means that classifying along the first two axes is more significant and peak normalization performed much better than the previous 5 normalization techniques.

In PCA, the correlation between a component and a variable (loading) estimates the information they share (Abdi and Williams, 2010). As shown in Figures 2 to 6, maximum and minimum temperatures can be considered as effective parameters in classification, while in peak normalization (Figure 7) their effect may be ignored. Therefore, $Mean_g$, $Mean_i$, $Mean_r$, $Mean_{gs}$, $Mean_b$, SD_b, SD_r, SD_i, and SD_{EG} were selected as classifying parameters that had the highest loadings, respectively. This result indicates that water stress in tomato plants can be determined using visible characteristics while no thermal image attributes performed as well, here. The classifying parameters were applied as the inputs of artificial neural networks.

3.2 Artificial neural networks

Multilayer perceptron neural network was applied as a supervised classification model. The network consisted of three (input, hidden, and output) layers. The 9 parameters, defined by PCA, were applied as the input neurons. The output layer was just 1 neuron that divided the output of multilayer perceptron neural networks (MLPNN) into two classes. The appropriate number of neurons for the hidden layer was found to be 10. This value was selected by trial and error and based on the lowest MSE value with the most r value (Table 2). Sigmoid transfer function and linear transfer function were applied in the hidden and output layers, respectively, and the network was trained using Levenberg-Marquardt algorithm (trainlm).

Table 2 Training, validation, and testing results of MLPNN on PCA outputs

N		MSE	r	N		MSE	r
1	Training	4.67301E-02	0.92	6	Training	1.81663E-04	0.99
	Validation	3.24114E-02	0.97		Validation	2.91178E-02	0.95
	Testing	5.76888E-02	0.90		Testing	1.48333E-01	0.70
2	Training	3.71195E-02	0.92	7	Training	1.58266E-02	0.97
	Validation	8.05059E-04	0.99		Validation	7.69647E-03	0.99
	Testing	5.15405E+00	0.99		Testing	2.80444E-02	0.96
3	Training	1.10604E-02	0.98	8	Training	2.53383E-04	0.99
	Validation	4.29477E-03	0.99		Validation	4.54109E-05	0.99
	Testing	6.55204E-03	0.99		Testing	1.87336E-02	0.96
4	Training	1.88066E-10	0.99	9	Training	1.52732E-02	0.98
	Validation	4.87744E-03	0.99		Validation	2.63993E-02	0.95
	Testing	7.69184E-02	0.85		Testing	3.31119E-02	0.93
5	Training	2.83429E-05	0.99	10	Training	2.60346E-03	0.99
	Validation	6.25578E-03	0.98		Validation	4.84167E-03	0.99
	Testing	1.77474E-02	0.98		Testing	6.04998E-03	0.99

Table 2 shows the results of MLPNN on the PCA outputs with hidden layer of 1 to 10 neurons. The overall correlations between the MLPNN-based classification and actual classes (succulent vs. water-stressed plants) show a good *r* of roughly 0.99 (Table 2). Rud et al. (2014) found *r*=0.99 for a thermal based water detection system in potatoes. Bellvert et al. (2014) reported the *r*=0.91 for water stress detection in vineyard using a thermal remote sensing imagery. The value of *r* was reported 0.91 in another research was done by Rossini et al. (2013) to map water stress in a maize field using hyperspectral remote sensing. Analyzing hyperspectral images to detect water stress in apple trees, Kim et al. (2011) found *r*=0.94.

In order to evaluate the accuracy of the developed classification algorithm, results of the developed algorithm were compared with a database of manually classified images. This algorithm was capable to classify the images in 83.3%. The error of the algorithm to classify normal and water-stressed plants was 26.7% and

6.7%, respectively. Therefore, the algorithm developed here performed better to work on water-stressed tomato plants rather than normal. The former error results in more water consumption by 26.7%; however, the 6.7% savings in water consumption due to the latter error, in the other hand, may reduce the productivity in water-stressed plants (Kim et al., 2011).

Although, in the reviewed literature, more emphasis has been placed on the thermal characteristics of a plant canopy, it was found that a classification algorithm based on visible features and MLPNN model (using the PCA-approved parameters of tomato canopy) yields better results here. Visible features can lead to the development of an inexpensive smart water stress detection system as opposed to spectral, or thermal-based algorithms developed by Kim et al. (2011), Sepulcre-Cantó et al. (2006), and Wang et al. (2010) which require much more expensive equipment. This algorithm is preferred to image segmentation methods used by Font et al. (2005) and Kacira et al. (2002), since it is not very complicated and does not require much processing time. Associated with low price, working with a visible camera is easier and its calibration for all the conditions takes a short time, making it appropriate to be utilized in commercial smart irrigation systems.

4 Conclusion

Among the 22 parameters applied on images for classifying to detect water-stressed tomato plants, nine parameters were determined to be most appropriate. The optimization process was implemented using Principal Components Analysis. Among the normalization methods, peak normalization performed better than the others with overall PCs of 99%. Peak normalization loading outputs were used in multilayer perceptron neural network to develop the classification algorithm. The outputs indicated $Mean_g$, $Mean_i$, $Mean_r$, $Mean_{gs}$, $Mean_b$, SD_b, SD_r, SD_i, and SD_{EG} to be the most appropriate parameters for classifying the images. All the parameters were extracted from visible light image characteristics.

Results of analysis showed that the classification algorithm was capable of detecting water stress based on nine visible properties of tomato plant canopy images (as input layer), 10 neurons in the hidden layer, and 1 neuron in the output layer. This approach can effectively be utilized for non-contact real-time determination of tomato irrigation requirements using an inexpensive camera. This is while the use of thermal images did not provide acceptable results. The overall accuracy of the developed algorithm to classify images to normal and water-stressed was 83.3%.

References

Abdi, H., and L. J. Williams. 2010. Principal component analysis. *Wiley Interdisciplinary Reviews: Computational Statistics*, 2(4): 433–459.

Anonymous. 2010. The Unscrambler Appendices: Method References. Trondheim, Norway: CAMO Software AS.

Bartzanas, T., Katsoulas, N., Elvanidi, A., Ferentinos, K.P. and Kittas, C., 2015, July. Remote sensing for crop water stress detection in greenhouses. In *10th European Conference on Precision Agriculture*, pp. 669-676. ECPA, Volcani Centre, Israel.

Bellvert, J., P. J. Zarco-Tejada, J. Girona, and E. Fereres. 2014. Mapping crop water stress index in a 'Pinot-noir'vineyard: comparing ground measurements with thermal remote sensing imagery from an unmanned aerial vehicle. *Precision Agriculture*, 15(4): 361–376.

Blum, A. 2011. Plant water relations, plant stress and plant production. In P*lant Breeding for Water-Limited Environments*, ed. A. Blum, ch. 1, 11-52. New York: Springer.

Casanova, J. J., S. A. O'Shaughness, S. R. Evett, and C. M. Rush. 2014. Development of a wireless computer vision instrument to detect biotic stress in wheat. *Sensors*, 14(9): 17753–17769.

Dinç, İ., M. Sigdel, S. Dinç, M. S. Sigdel, M. L. Pusey, and R. S. Aygün. 2014. Evaluation of normalization and PCA on the performance of classifiers for protein crystallization images. In *IEEE SOUTHEASTCON*, 1–6. Lexington, KY, USA, 13-16 March.

Font, L., F. Korosi, and I. Farkas. 2005. Leaf inclination based non destructive water stress indication for vegetables. *Acta Horticulturae*, 691(1): 99.

Heuvelink, E. 2005. *Tomatoes*. *Crop Production Science in Horticulture Series 13*. Wallingford, UK: CABI Publishing.

Holland, S. M. 2008. *Principal Components Analysis (PCA)*. p1-10. Department of Geology, University of Georgia, Athens, GA.

Kacira, M., P. P. Ling, and T. H. Short. 2002. Machine vision

extracted plant movement for early detection of plant water stress. *Transactions of the ASAE*, 45(4): 1147–1153.

Katsoulas, N., A. Elvanidi, K. P. Ferentinos, M. Kacira, T. Bartzanas, and C. Kittas. 2016. Crop reflectance monitoring as a tool for water stress detection in greenhouses: A review. *Biosystems Engineering*, 151: 374–398.

Kim, Y., D. M. Glenn, J. Park, H. K. Ngugi, and B. L. Lehman. 2011. Hyperspectral image analysis for water stress detection of apple trees. *Computers and Electronics in Agriculture*, 77(2): 155–160.

Lin, K., J. Chen, H. Si, and J. Wu. 2013. A review on computer vision technologies applied in greenhouse plant stress detection. In *IGTA Chinese Conference on Image and Graphics Technologies*, 192–200. Beijing, China, 2-3 April.

López., A., F. D. Molina-Aiz, D. L. Valera, and A. Peña. 2012. Determining the emissivity of the leaves of nine horticultural crops by means of infrared thermography. *Scientia Horticulturae*, 137: 49–58.

Ondimu, S. N., and H. Murase. 2008. Comparison of plant water stress detection ability of color and gray-level texture in Sunagoke moss. *Transactions of the ASABE*, 51(3): 1111–1120.

Park, L. A. F. 2011. Fast approximate text document clustering using compressive sampling. In *Joint European Conference on Machine Learning and Knowledge Discovery in Databases*, 565–580. Athens, Greece, 5-9 September.

Rossini, M., F. Fava, S. Cogliati, M. Meroni, A. Marchesi, C. Panigada, C.Giardino, L. Busetto, M. Migliavacca, S.

Wolf, S., and J. Rudich. 1988. The growth rates of fruits on different parts of the tomato plant and the effect of water stress on dry weight accumulation. *Scientia Horticulturae*, 34(1-2): 1–11.